



In vivo selective imaging and inhibition of leukemia stem-like cells using the fluorescent carbocyanine derivative, DiOC5(3)



Beibei Zhang^{a,1}, Yasuhito Shimada^{a,b,c,d,e,1}, Junya Kuroyanagi^a, Michiko Ariyoshi^a, Tsuyoshi Nomoto^f, Taichi Shintou^f, Noriko Umemoto^{a,b}, Yuhei Nishimura^{a,b,c,d,e}, Takeshi Miyazaki^f, Toshio Tanaka^{a,b,c,d,e,*}

^a Department of Molecular and Cellular Pharmacology, Pharmacogenomics and Pharmacoinformatics, Mie University Graduate School of Medicine, 2-174 Edobashi, Tsu, Mie 514-8507, Japan

^b Department of Systems Pharmacology, Mie University Graduate School of Medicine, 2-174 Edobashi, Tsu, Mie 514-8507, Japan

^c Mie University Medical Zebrafish Research Center, 2-174 Edobashi, Tsu, Mie 514-8507, Japan

^d Department of Bioinformatics, Mie University Life Science Research Center, 2-174 Edobashi, Tsu, Mie 514-8507, Japan

^e Department of Omics Medicine, Mie University Industrial Technology Innovation, 2-174 Edobashi, Tsu, Mie 514-8507, Japan

^f Corporate R&D Headquarters, Canon Inc, Ohta-ku, Tokyo 146-8501, Japan

ARTICLE INFO

Article history:

Received 17 November 2014

Received in revised form

14 January 2015

Accepted 1 February 2015

Available online 21 February 2015

Keywords:

Xenotransplant

Zebrafish

Leukemia stem cell

High-throughput screening

ABSTRACT

Elimination of leukemia stem cells (LSCs) is necessary for the destruction of malignant cell populations. Owing to the very small number of LSCs in leukemia cells, xenotransplantation studies are difficult in terms of functionally and pathophysiologically replicating clinical conditions of cell culture experiments. There is currently a limited number of lead compounds that target LSCs. Using the LSC-xenograft zebrafish screening method we previously developed, we found that the fluorescent compound 3,3'-dipentylloxycarbocyanine iodide (DiOC5(3)) selectively marked LSCs and suppressed their proliferation *in vivo* and *in vitro*. DiOC5(3) had no obvious toxicity to human umbilical cord blood CD34+ progenitor cells and normal zebrafish. It accumulated in mitochondria through organic anion transporter polypeptides that are overexpressed in the plasma membrane of LSCs, and induced apoptosis via ROS overproduction. DiOC5(3) also inhibited the nuclear translocation of NF- κ B through the downregulation of LSC-selective pathways, as indicated from DNA microarray analysis. In summary, DiOC5(3) is a new type of anti-LSC compound available for diagnostic imaging and therapeutics that has the advantage of being a single fluorescent chemical.

© 2015 Elsevier Ltd. All rights reserved.

1. Introduction

Increasing evidence indicates that leukemia stem cells (LSCs) are initiators of the occurrence, development and recurrence of hematologic malignancies [1]. LSCs also represent a malignant reservoir of disease-causing cells that is believed to drive relapse and resistance to chemotherapy [2]. Targeting LSCs would provide a less toxic approach than regular chemotherapeutic agents that kill in bulk, rapidly proliferating cancer cells and normal cells that

* Corresponding author. Department of Molecular and Cellular Pharmacology, Pharmacogenomics and Pharmacoinformatics, Mie University Graduate School of Medicine, 2-174 Edobashi, Tsu, Mie 514-8507, Japan. Tel.: +81 59 231 5411; fax: +81 59 232 1765.

E-mail address: tanaka@doc.medic.mie-u.ac.jp (T. Tanaka).

¹ Contributed equally to this work.

divide rapidly [3]. To date, major research efforts have been aimed at identifying and eradicating the LSC population in leukemia [2]. For example, high expression of aldehyde dehydrogenase (ALDH) in LSCs has been successfully applied to identify LSCs in clinical practice [4,5].

In recent years, zebrafish have been proposed as a cost-effective alternative to human disease models to assess the efficacy and toxicity of chemical compounds in a high-throughput manner [6,7]. For example, their small size makes it possible to do 96-well plate experiments. Furthermore, because of their transparent body wall, *in vivo* imaging is possible in this model. For these reasons, zebrafish have also been utilized in cancer research and drug screening for over a decade [8–10]. The immaturity of the young zebrafish immune system allows the xenotransplantation of human cancer cells into the fish as early as 48 h postfertilization (hpf) [11]. By taking advantage of the unique features provided by the zebrafish

model for understanding cancer progression, breast cancer stem-like cells and glioma stem cells xenografted into zebrafish have been explored to reveal the mechanism of cancer stem cell (CSC) development [12,13]. In addition, we also have developed a screening system using LSC xenograft zebrafish for discovery of LSC selective inhibitors [14,15].

Fluorescent chemicals themselves and their conjugated molecules (i.e., antibodies) have been widely used for the visualization of cellular organelles and analysis of their functions *in vitro* [16,17] and *in vivo* [18–20]. For CSC research, the *in vivo* visualization of CSC enables the real-time evaluation of drug response in animal testing and human clinical trials. In fact, there are few fluorescent chemicals that can selectively label CSC [21,22]. However, there is no CSC-targeted fluorophore with selective cytotoxic ability, except for conjugated antibodies, that would offer a novel therapeutic strategy to combine drug testing and CSC eradication. In this study, we conducted drug screening from a fluorescent chemical library using LSC xenograft zebrafish, and found that the lipophilic cationic carbocyanine 3,3'-dipentylloxycarbocyanine iodide, DiOC5(3), labeled LSCs selectively and inhibited their proliferation.

2. Materials and methods

2.1. Ethical approval

All animal experiments were conducted according to the Animal Welfare and Management Act (Ministry of Environment of Japan) and complied with international guidelines. After the experiments, the fish were killed by an overdose of anesthesia.

2.2. Compounds

All fluorescent compounds examined in this study were obtained from Canon Inc. (Tokyo, Japan). The stock solutions (10 mM) were dissolved in dimethyl sulfoxide (Nacalai Tesque, Kyoto, Japan). Imatinib mesylate, BSP, NAC and IKK inhibitor BMS-345541 were purchased from Sigma–Aldrich (St. Louis, MO, USA). IKK γ NEMO Binding Domain (NBD) Inhibitory Peptide was purchased from Novus Biologicals (Imgenex, San Diego, CA, USA). For anesthesia, 100 ppm 2-phenoxyethanol (Wako Pure Chemical Industries, Osaka, Japan) was diluted in E3 medium (5 mM NaCl, 0.17 mM KCl, 0.4 mM CaCl₂, and 0.16 mM MgSO₄).

2.3. Cell culture and fluorescent labeling

K562 cells were obtained from the RIKEN Cell Bank (Tokyo, Japan) and pre-cultured in RPMI1640 medium (Life Technologies, Carlsbad, CA, USA) supplemented with 10% heat inactivated fetal bovine serum (FBS; Life Technologies), 100 U penicillin G (Sigma–Aldrich)/ml and 100 μ g streptomycin (Sigma–Aldrich)/ml at 37 °C in 5% CO₂. The K562 cells stably expressing Kusabira-Orange (KOr) fluorescent protein (K562-KOr cells) were prepared as described previously [14].

2.4. LSCs isolation

The subpopulations of ALDH high expression (ALDH⁺) and low expression (ALDH⁻) from K562 or K562-KOr cells were sorted in an ALDEFUOR assay (STEMCELL Technologies, Vancouver, Canada) followed by FACS Aria flow cytometry (BD Biosciences, San Jose, CA, USA), according to the manufacturer's instructions.

2.5. Cell proliferation assay

ALDH⁺ and ALDH⁻ cells were cultured in 96-well plates at a density of 3000 cells per well in RPMI1640 medium (Life Technologies) supplemented with 1% FBS (Life Technologies), 100 U penicillin G/ml and 100 μ g streptomycin/ml (Sigma–Aldrich) at 37 °C in 5% CO₂. After treatment with the tested compounds, cell proliferation was measured using the CellTiter-Glo luminescent cell viability assay (Promega, Madison, WI, USA). Luminescence signals were measured in a Victor2 fluorescent plate reader (PerkinElmer, Boston, MA, USA).

2.6. Intracellular ROS quantification

Intracellular ROS status was measured using a superoxide detection reagent (ENZO Life Science, Ann Arbor, MI, USA). The cells were treated with 1 μ M reagent for 60 min at 37 °C in 5% CO₂, and washed three times with phosphate-buffered saline (PBS). Following a 5 min nuclear staining by 40 μ g/ml Hoechst 33342 solution (Dojin, Kumamoto, Japan), the images were captured using the ImageXpress Micro high-content screening system (Molecular Devices, Sunnyvale, CA, USA). Cell fluorescence was quantified using the accompanying software.

2.7. Mitochondrial and ER imaging

ALDH⁺ and ALDH⁻ cells were treated with fluorescent chemicals (200 nM, 24 h) and stained with 200 nM MitoTracker Red CMXRos (Molecular Probes, Carlsbad, CA, USA) for 15 min at 37 °C in 5% CO₂. After removing labeling solution, three washes were performed with fresh pre-warmed medium and images were captured using a Zeiss LSM 510 confocal microscope (Carl Zeiss, Thornwood, NY, USA) and the ImageXpress MICRO high content screening system (Molecular Devices). Similar protocols were performed with 1 μ M ER-Tracker Blue–White DPX for ER staining (Molecular Probes).

2.8. Detection of apoptotic cells

ALDH⁺ and ALDH⁻ cells were treated with candidate chemicals. The Deadend Colorimetric TUNEL System (Promega) was used to visualize the apoptotic cells according to the manufacturer's instructions. The images were captured using the Axiocvert 200M microscope (Carl Zeiss).

2.9. siRNA transfection

The cells were transfected with the stealth siRNAs (10620318/10620319-254487 H01-06 for *SLOC4A1*; 10620318/10620319-259553 B07-12 for *SLCO4C1*; Life Technologies) using Lipofectamine RNAiMAX (Life Technologies) according to the manufacturer's instructions. For siRNA targeting of two genes, the combinations of H01-02 and B07-08, H03-04 and B09-10, H05-06 and B11-12 were used. Seventy-two hours after transfection, cells were used for the experiments.

2.10. Zebrafish

Care and breeding of zebrafish were performed by following protocols as described previously [23]. In this study, we used *nacre/rose/fli1:egfp* zebrafish, which was obtained by cross-breeding *nacre*^(-/-)/*rose*^(-/-) mutants and Tg (*fli1:egfp*) transgenic zebrafish as described previously [14]. The high degree of transparency of zebrafish allowed for *in vivo* monitoring of tumor angiogenesis.

2.11. Leukemia cell xenotransplantation

The xenotransplantation procedures were described in our previous study [14]. In brief, just before xenotransplantation, 48-hpf zebrafish were dechorionated using 2 mg pronase (Roche Diagnostics)/ml, anesthetized with 2-phenoxyethanol solution (100 ppm; Wako Pure Chemical Industries), and arrayed on a holding sheet. ALDH⁺ and ALDH⁻ cells (1 \times 10⁶ cells each) were separately suspended in 50 μ l of Hanks' balanced salt solution (Life Technologies). The avascular region of the yolk sac was then injected with 100–200 cells using the glass needles and the Femtojet injection system (Eppendorf, Hamburg, Germany).

2.12. Zebrafish high-content imaging and analysis

Twenty-four hours after xenotransplantation (72 hpf), zebrafish were anesthetized with 2-phenoxyethanol solution (100 ppm; Wako Pure Chemical Industries). The successfully xenotransplanted zebrafish were selected by a MZ16F stereoscopic microscope (Leica Microsystems, Wetzlar, Germany) equipped with the GFP3 (for EGFP) and DsRed (for KOr) filters and a DP71 digital camera (Olympus, Tokyo, Japan). Then, they were transferred in 50 μ l of anesthetic solution into a 96-well imaging plate (BD Biosciences). The images were captured using the ImageXpress MICRO high content screening system (Molecular Devices) and quantified using the accompanying software according to the previous study [14].

2.13. Chemical treatment to cancer xenotransplanted zebrafish

After initial imaging of the fish, a JANUS automated workstation (Perkin–Elmer, Waltham, MA, USA) was used to replace the anesthetic solution with 100 μ l of the test compound in E3 medium. The 96-well plate was shaken for 30 s on an MTS2 shaker (IKA Labortechnik, Staufen, Germany) and then incubated at 32 °C as described above. After 24 h, the medium was replaced with fresh chemical-containing medium using the JANUS automated workstation. Forty-eight hours after treatment (120 hpf), the zebrafish were imaged again as described above. As for the dye injection, 30 nl dye (10 μ M) was injected into the yolk sac of zebrafish using the glass needles and the Femtojet injection system above (Eppendorf).

2.14. Total RNA extraction, cDNA synthesis, and q-PCR

Total RNA was extracted from the cells using the RNeasy Mini kit (Qiagen, Hilden, Germany) according to the manufacturer's instructions. The first-strand cDNA was synthesized from 200 ng of total RNA using the SuperScript III cDNA synthesis kit (Life Technologies) with random primers (Life Technologies). The q-PCR was performed using Power SYBR Green Master Mix (Applied Biosystems, Foster City, CA, USA) and a 7300 Real-time PCR system (Applied Biosystems) as recommended by the manufacturer. The primers shown in Supplementary Table S3 were used to amplify target genes.

2.15. NF- κ B detection

The NF- κ B activity in the nucleus was analyzed using the NF- κ B filter plate assay (Signosis, Santa Clara, CA, USA). Luminescence is reported as relative light units using the Varioskan Flash Multimode Plate Reader (Thermo Scientific, Waltham, MA, USA).

2.16. Western blot

Cellular extracts were prepared using Cell Lysis Buffer (Abcam, Cambridge, MA, USA). Protein concentration was determined using a Bradford Ultra Protein Assay Kit (Expendon, Cambridge, UK). Protein samples (30 μ g) were heated to 70 °C for 10 min and separated on a 4–12% Bis-Tris gel using a NuPAGE SDS-PAGE Gel System (Life Technologies). Separated proteins were then transferred to polyvinylidene difluoride (PVDF) membranes (iBlot PVDF; Life Technologies) and blocked in PVDF Blocking Reagent (Toyobo, Osaka, Japan). Following blocking, blots were incubated in Can Get Signal Immunoreaction Enhancer Solution 1 (Toyobo), containing primary antibody, overnight at 4 °C, followed by three 10 min washes with PBS containing Tween 20 (PBST). Polyclonal anti-phosphor-IKK α / β (Ser175/180) (1:1000 dilution; Cell Signaling Technology, Beverly, MA, USA), anti-phosphor-IKK γ (Ser376) (1:1000; Cell Signaling Technology), anti-26S proteasome (1:1000; Abcam), and anti-Actin (1:2000; Abcam) antibodies were used. The washed membrane was incubated in Can Get Signal Immunoreaction Enhancer Solution 2 (Toyobo) containing Alexa Fluor 488-labeled anti-rabbit IgG (1:1000; Sigma–Aldrich) and anti-mouse IgG (1:1000; Sigma–Aldrich) for 1 h at 25 °C. After three washes with PBST, the bound antibodies were visualized using a Typhoon 9410 high performance laser scanning system (GE Healthcare, Waukesha, WI, USA). Gel images were analyzed using ImageQuant Tools Software (GE Healthcare).

2.17. DNA microarray analysis

Total RNAs were extracted from the ALDH+/- subpopulations of K562 cells with or without 200 nM DiOC5(3) treatment for 24 h. The hybridized microarrays were prepared using Agilent Whole Human Genome Oligo Microarrays (G4112F) according to the manufacturer's protocol, then scanned by an Agilent Microarray Scanner G2565BA and analyzed using Feature Extraction software (Agilent Technologies, Santa Clara, CA, USA). The significant genes that exhibited at least a 2-fold change were included. Using the Life Science Knowledge Bank (World Fusion, Tokyo, Japan) and Pathway Studio 9.0 (Ariadne Genomics, Rockville, MD, USA), Gene ontology (GO) term method analysis and SNEA ($P < 0.05$, FDR < 0.25) were performed [24,25].

2.18. Statistical analysis

Data were analyzed using statistical package SPSS 19.0 (SPSS, Chicago, IL, USA). Differences between the two groups were examined for statistical significance by the independent Student's t-test. For multiple comparisons, the assessments were analyzed by one-way analysis of variance followed by a Bonferroni-Dunn multiple comparison test. All data were expressed as mean plus or minus standard error of the mean. Values were considered to be significant when $P < 0.05$.

3. Results

3.1. Zebrafish xenograft screening identified DiOC5(3) as a LSC inhibitor

A chemical screening of 336 fluorescent compounds was conducted to identify compounds that produce LSC selective inhibition and staining using human chronic myelogenous leukemia (CML) K562 cells xenografted in zebrafish as described previously [14]. In brief, the K562 ALDH+/- cells were first xenotransplanted into the yolk sac of 2-days-postfertilization (dpf) zebrafish and then treated with test chemicals for 48 h from 24 h postinjection (hpi), and their proliferation was evaluated *in vivo* by cancer fluorescence. The ALDH+ population of K562 cells is thought to be a putative LSC population based on previous studies [4,5,14]. As a result of the screening, we focused on 3,3'-dipentylloxycarbonyl iodide (DiOC5(3)) as a LSC-selective dye. Representative images of xenografts exposed to DiOC5(3) or imatinib (a control anti-leukemia drug) are depicted in Fig. 1A. Both of them significantly inhibited ALDH- cell proliferation after 48 h exposure at 0.5 μ M ($P < 0.01$ vs. control; Fig. 1B). However, DiOC5(3) inhibited ALDH+ cell proliferation selectively compared with ALDH- cells ($P < 0.05$), in contrast to imatinib which showed LSC-resistance. We also injected

DiOC5(3) into the yolk sac of the xenograft zebrafish of 24 hpi. After 1 h of dye injection, DiOC5(3) can visualize the ALDH+ cells rather than ALDH- cells *in vivo* (Fig. 1C and D). ALDH+ cells were also decreased more than ALDH- cells during 48 h after DiOC5(3) injection (Fig. 1E). In addition, ALDH+ cells sometimes migrated from the implanted region, and injected DiOC5(3) could stain these migrated cells clearly (Supplementary Fig. S1).

3.2. DiOC5(3) selectively stained LSCs and inhibited their proliferation *in vitro*

A cell-based assay was conducted to evaluate the DiOC5(3) effects on LSC staining and proliferation. DiOC5(3) was incorporated into ALDH+ cells at a significantly higher rate than ALDH- cells and human umbilical cord blood (HUCB) CD34+ progenitor cells ($P < 0.01$, respectively; Fig. 2A and B). DiOC5(3) also suppressed the cell proliferation of ALDH+ cells to a significantly higher degree than ALDH- cells and HUCB CD34+ progenitor cells ($P < 0.01$, respectively; Fig. 2C). In addition, DiOC5(3) was able to suppress ALDH+ cell proliferation more than ALDH- cells in K562 cells in a dose-dependent manner (IC50 for K562 ALDH+ is 0.29 μ M and K562 ALDH- is 0.68 μ M, $P < 0.05$ vs. ALDH-; Supplementary Fig. S2A), contrary to the results showing ALDH+ cell resistance to imatinib (IC50 for K562 ALDH+ is 0.52 μ M and K562 ALDH- is 0.24 μ M, $P < 0.05$ vs. ALDH-; Supplementary Fig. S2B). For the other leukemia cell lines KU812E and NCO2, DiOC5(3) was also incorporated into ALDH+ cells significantly more than ALDH- cells (Supplementary Fig. S3A for 30 min, and S3 B for 48 h treatment). Furthermore, the proliferation of ALDH+ cells was also suppressed more than ALDH- cells (Supplementary Fig. S3C) after 48 h treatment. We also evaluated the effects of DiOC5(3) analogs to K562 ALDH+ cells (Fig. 2D).

To evaluate the DiOC5(3) effects on non-cancer cells, we added DiOC5(3) to the zebrafish embryo-derived cells and adult zebrafish blood cells (ZBCs). DiOC5(3) does not stain zebrafish cells (data not shown). For cell proliferation, DiOC5(3) exhibited cytotoxicity in ZBCs and HUCB CD34+ progenitor cells, with a higher concentration than in K562 cells (IC50 for ZBC is 1.10 μ M, HUCB CD34+ is 2.03 μ M; Supplementary Fig. S4A and B). Regarding developmental toxicity, zebrafish embryos exhibited no death with 1 μ M DiOC5(3) administration from 48 hpf for 48 h (Supplementary Fig. S4C). There was no phenotypic change detected unless green-fluorescent staining was present throughout the whole body (Supplementary Fig. S4D).

3.3. The mechanism of DiOC5(3) uptake in K562 cells

Using confocal microscopy, DiOC5(3) was detected accumulating in the mitochondria of K562 ALDH+/- cells (Fig. 3A). To investigate the mechanism of the DiOC5(3) uptake, ALDH+ cells were pre-incubated with 250 μ M sulfobromophthalein (BSP), a competitive inhibitor of organic anion transporting polypeptides (OATPs), for 10 min before DiOC5(3) treatment. The accumulation of DiOC5(3) was almost completely inhibited by pre-treatment with BSP (Fig. 3B). Among OATP family members, *SLC04A1* and *SLC04C1* expression levels were significantly higher in ALDH+ cells than ALDH- cells ($P < 0.01$, $P < 0.05$ respectively; Fig. 3C). Double knockdown of *SLC04A1* and *SLC04C1* significantly suppressed DiOC5(3) uptake ($P < 0.01$; Fig. 3D and E), and recovered the cell proliferation of ALDH+ cells ($P < 0.05$ vs. negative siRNA treatment) under the DiOC5(3) treatment (Fig. 3F). *SLC04A1* knockdown alone also significantly suppressed the DiOC5(3) uptake in ALDH+ cells ($P < 0.01$; Supplementary Fig. S5A and B); however, the level of cell proliferation was not recovered.

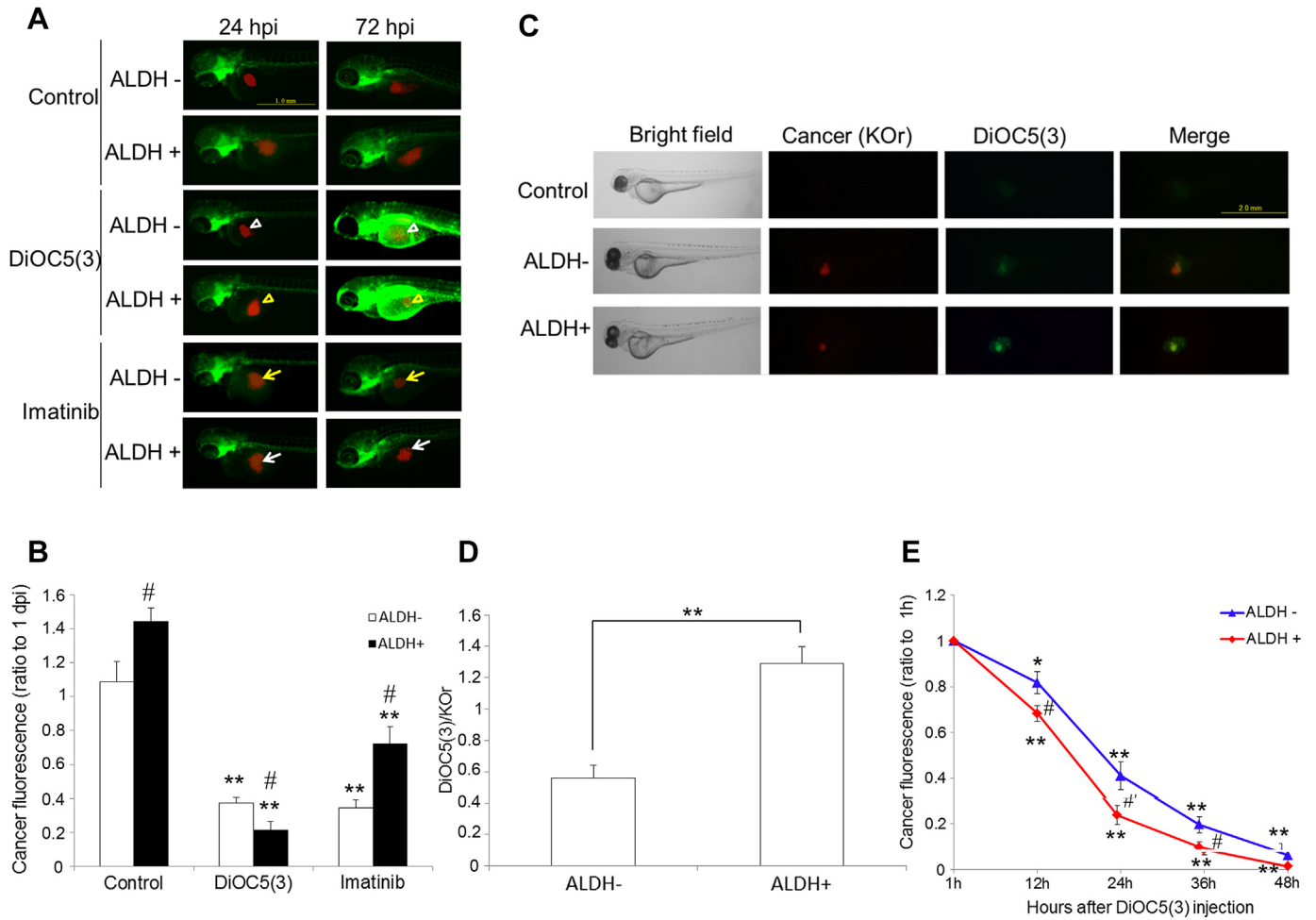


Fig. 1. DiOC5(3) selectively inhibits LSC proliferation in zebrafish xenograft. (A) Representative images of xenograft zebrafish with DiOC5(3) or imatinib (control anti-leukemia drug) treatment. DiOC5(3) suppressed the cancer proliferation in the ALDH+ xenograft (yellow arrowhead) more than in the ALDH- xenograft (white arrowhead). In contrast, imatinib suppressed the cancer proliferation in the ALDH- xenograft (yellow arrow) more than in ALDH+ xenograft (white arrow). (B) Quantification of tumor proliferation by cancer KOR-fluorescence. The chemicals (0.5 μM) were administered during 1–2 dpi (3–4 dpf). A total of 15–25 embryos were used per condition and the average of three experiments was shown (n was used to indicate the fish number below). # $P < 0.05$ vs. ALDH- cells; ** $P < 0.01$ vs. control. (C) DiOC5(3) (10 μM , 30 nl) was injected into the yolk sac of 1 dpi-xenografts and images were captured 1 h after the dye injection. ALDH+ cells were strongly stained with DiOC5(3), compared with ALDH- cell xenograft. (D) Quantification of tumor staining with DiOC5(3). $n = 8$, ** $P < 0.01$. (E) DiOC5(3) injection inhibited cancer proliferation in xenograft zebrafish. $n = 8$, * $P < 0.05$, ** $P < 0.01$ vs. 1 h after DiOC5(3) injection; # $P < 0.05$ vs. ALDH- cells. (For interpretation of the references to color in this figure legend, the reader is referred to the web version of this article.)

3.4. DiOC5(3) induced apoptosis with ROS overproduction in ALDH+ cells

DiOC5(3) inhibits bovine heart mitochondrial respiration through inhibition of NADH-ubiquinone reductase activity in respiratory complex I [26]. NADH-ubiquinone reductase catalyzes the reaction from NADH to NAD^+ during the process of electron transport [27]. We also found that DiOC5(3) significantly increased the NADH/ NAD^+ ratio in isolated mitochondria ($P < 0.05$; Fig. 4A), suggesting that DiOC5(3) could inhibit NADH-ubiquinone reductase activity also in K562 cells. Since NADH-ubiquinone reductase is highly involved in ROS production [28], we next evaluated the DiOC5(3) effects on intracellular ROS levels of K562 subpopulations (Fig. 4B). Without DiOC5(3) treatment, the ROS level of ALDH+ cells was lower than that of ALDH- cells ($P < 0.01$; Fig. 4C). After 200 nM DiOC5(3) treatment for 24 h, intracellular ROS level of both cells was increased ($P < 0.01$; Fig. 4C), whereas the increased ratio in ALDH+ cells was higher. Subsequent to the ROS elevation, the apoptotic cells were increased in DiOC5(3) treated K562 ALDH+/- cells ($P < 0.01$; Fig. 4D and E). The ALDH+ cells were more sensitive

to DiOC5(3) than ALDH- in terms of apoptotic response ($P < 0.01$ vs. ALDH-; Fig. 4E).

We analyzed the CML marker *BCR-ABL*, CSC markers *SIRT1*, *CD44* and *CD133*, the anticancer genes *TP53(p53)* and *CDKN1A(p21)* in K562 ALDH+/- cells (Fig. 4F–K). We found that *BCR-ABL*, *SIRT1*, *CD44* and *CD133* were higher, whereas *TP53* and *CDKN1A* were lower in ALDH+ cells compared with ALDH- cells ($P < 0.01$; Fig. 4F–K). DiOC5(3) treatment downregulated the *BCR-ABL*, *SIRT1*, *CD44* and *CD133* in both ALDH+ and ALDH- cells ($P < 0.01$ or $P < 0.05$; Fig. 4F–K), and upregulated the expression of the anti-cancer genes, *TP53* and *CDKN1A* ($P < 0.01$; Fig. 4J and K).

3.5. DiOC5(3) selectively inhibited NF- κ B nucleus localization in ALDH+ cells

DiOC5(3)-induced ROS overproduction was blocked by the addition of the antioxidant N-acetylcysteine (NAC) (Supplementary Fig. S6A and B). However, the ROS reduction did not recover the DiOC5(3)-induced proliferation completely (Supplementary Fig. S6C). This implied that the damage caused by DiOC5(3) was

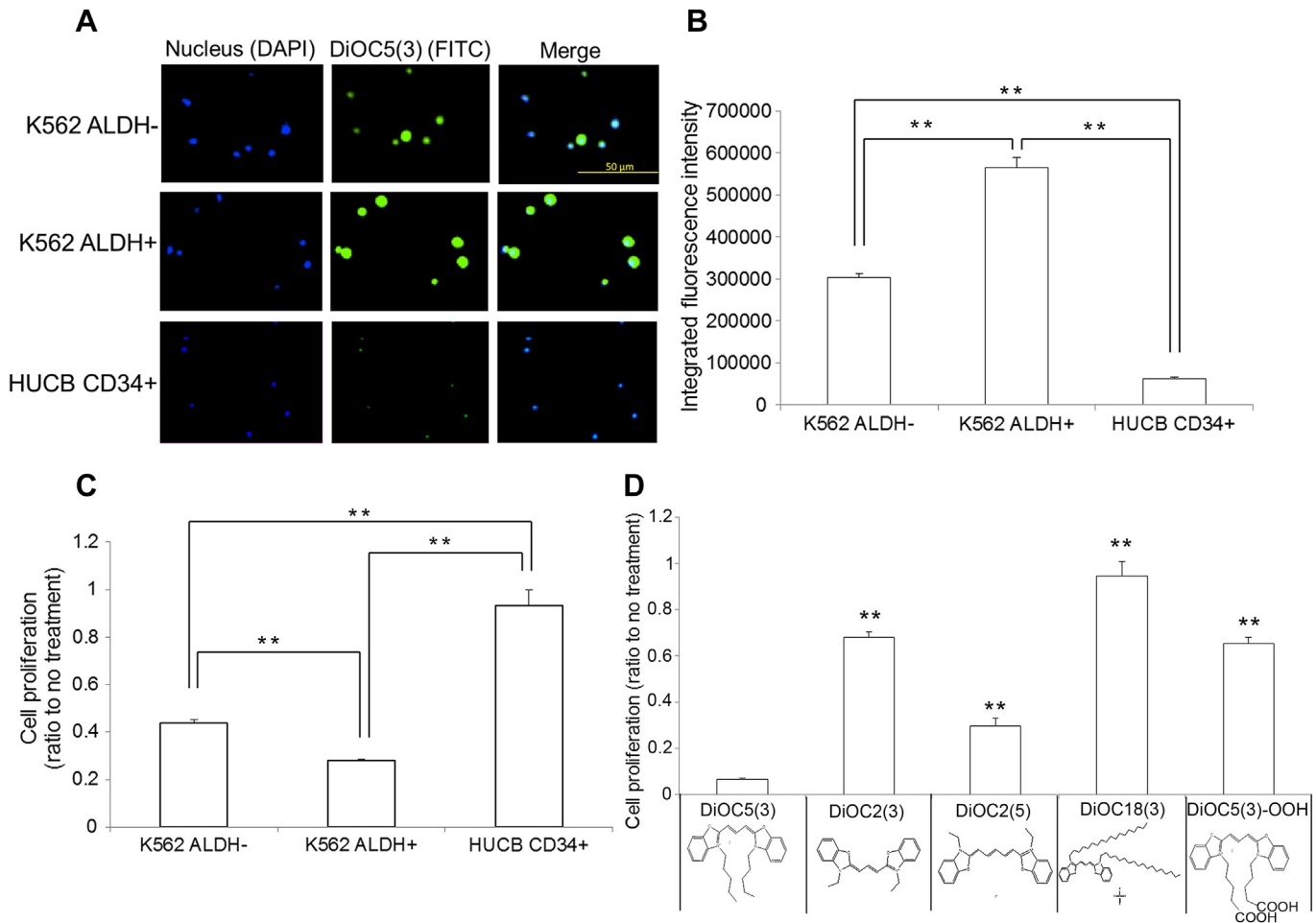


Fig. 2. DiOC5(3) selectively stains LSCs and inhibited their proliferation *in vitro*. (A) Representative images of K562 ALDH^{-/+} cells and HUCB 34⁺ progenitor cells with DiOC5(3) treatment (300 nm, 48 h). DAPI filter is for the nuclei staining by Hoechst 33342, and the FITC filter is for the DiOC5(3). (B) Quantification of DiOC5(3) fluorescence. DiOC5(3) accumulated in K562 ALDH⁺ cells more than in ALDH⁻ ones. Also, HUCB CD34⁺ cells showed less DiOC5(3) than K562 cells. $n = 4$, $**P < 0.01$. (C) Cell proliferation of ALDH^{-/+} cells and HUCB 34⁺ progenitor cells with DiOC5(3) treatment (300 nm, 48 h). $n = 4$, $**P < 0.01$. (D) Cell proliferation of K562 ALDH⁺ cells treated by DiOC5(3) analogs (10 μM , 24 h). $n = 4$, $**P < 0.01$ vs. DiOC5(3).

not only because of ROS overproduction in mitochondria. Since NF- κ B activity plays an important role in LSCs as one of major drug targets [29–31], we evaluated the NF- κ B activity in DiOC5(3)-treated K562 cells. The nuclear translocation of NF- κ B was inhibited by DiOC5(3) in ALDH⁺ cells to a greater degree than in ALDH⁻ cells (Fig. 5A). In addition, the NF- κ B downstream *SOD1* and *SOD2* expression were downregulated by DiOC5(3) treatment ($P < 0.05$; Fig. 5B and C). The expression levels of *NF- κ B1* and *NF- κ B2* mRNA in ALDH⁺ cells were lower than in ALDH⁻ cells, and DiOC5(3) increased their expressions (Supplementary Fig. S7A and B). In addition, the *NF- κ B1* expression was higher than *NF- κ B2* in K562 ALDH⁺ cells, but not in ALDH⁻ cells ($P < 0.01$; Supplementary Fig. S7C). DiOC5(3) treatment also upregulated IKK β and IKK γ (NEMO) expression, which signal to the kinase complex to activate the NF- κ B pathway [32–34] (Supplementary Fig. S7D and E). The IKK- β selective inhibitor, BMS-345541, and IKK γ NEMO Binding Domain (NBD) inhibitory peptide, which inhibit mainly the NF- κ B canonical pathway [35,36], showed selective inhibition to ALDH⁺ cells (BMS-345541: IC₅₀ for K562 ALDH⁺ is 6.39 μM , ALDH⁻ is 12.75 μM ; NBD inhibitory peptide: IC₅₀ for K562 ALDH⁺ is 40.52 μM , ALDH⁻ is 62.38 μM ; Supplementary Fig. S7F and G). Since DiOC5(3) was reported to accumulate in the endoplasmic reticulum (ER) [37], we also confirmed its ER staining in K562 subpopulations (Fig. 5D). 26S proteasome, produced in the ER, plays a key role in

the ubiquitination and proteosomal degradation process in canonical NF- κ B activation [32]. Western blot analysis showed that DiOC5(3) significantly reduced the 26S proteasome, which is highly expressed in K562 ALDH⁺ cells ($P < 0.01$; Fig. 5E and F). The phosphorylation of IKK $\alpha/\beta/\gamma$ subunits were also significantly reduced by DiOC5(3) treatment ($P < 0.05$, $P < 0.01$ respectively; Supplementary Fig. S7H and I).

3.6. Transcriptome analysis of DiOC5(3)-treated K562 subpopulations

We compared the genome-wide expression profiles of K562 ALDH⁺ and ALDH⁻ cells with or without DiOC5(3) to identify genes related to selective inhibition of LSCs. Gene ontology (GO) analysis was used to identify differences between ALDH⁺ and ALDH⁻ in major cellular processes. The GO results were listed in Table S1 for cell-subpopulations independently, and Table S2 for LSC-specific subpopulations. Fig. 6A shows the numbers of genes altered by DiOC5(3), which were highly involved in stress response/apoptosis, cell differentiation, DNA replication, DNA repair and cell cycle. These alternations were exaggerated in ALDH⁺ cells rather than ALDH⁻ cells. To predict the site of action of the therapeutic effects of DiOC5(3), we conducted Sub-Network Enrichment Analysis (SNEA) of our DNA microarray data [38]. Fig. 6B shows the

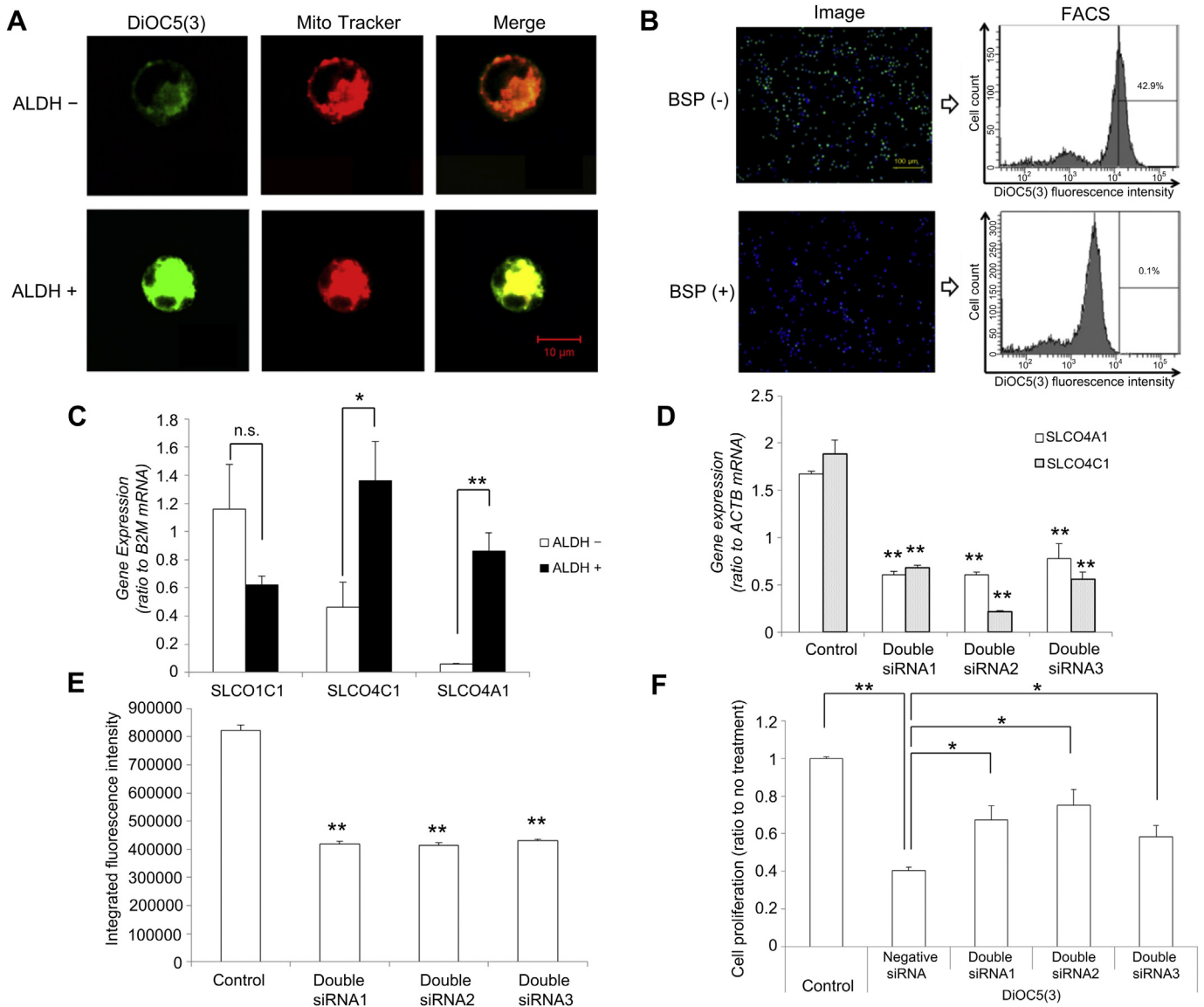


Fig. 3. DiOC5(3) accumulates in mitochondria of leukemia cells. (A) Confocal images of K562 ALDH^{-/-} cells with DiOC5(3) (green) and MitoTracker Red CMXRos (red). In ALDH⁺ cells, DiOC5(3) and MitoTracker Red were highly co-localized (yellow) in mitochondria. (B) Pretreatment with BSP (250 μ M, 10 min), a competitive inhibitor of OATPs, inhibited DiOC5(3) (200 nM, 10 min) uptake in K562 ALDH⁺ cells (left: microscopic images, and right: FACS analysis). Blue, Hoechst 33342 (nucleus), and green, DiOC5(3). (C) mRNA expression of OATP family members, *SLCO1C1*, *SLCO4C1* and *SLCO4A1*, in K562 ALDH^{-/-} cells. $n = 3$, n.s., not significant, * $P < 0.05$, ** $P < 0.01$. (D) Double knockdown of *SLCO4A1* and *SLCO4C1* in K562 ALDH⁺ cells. $n = 3$, *** $P < 0.001$ vs. each control. (E) Double knockdown of *SLCO4A1* and *SLCO4C1* decreased the DiOC5(3) uptake (500 nM, 24 h) in K562 ALDH⁺ cells. $n = 4$, ** $P < 0.01$. (F) Double knockdown of *SLCO4A1* and *SLCO4C1* recovered cytotoxicity of K562 ALDH⁺ cells treated with DiOC5(3) (500 nM, 24 h). $n = 4$, * $P < 0.05$; ** $P < 0.01$. (For interpretation of the references to color in this figure legend, the reader is referred to the web version of this article.)

comparison between ALDH⁺ and ALDH⁻ cells following DiOC5(3) treatment. Though DiOC5(3) treatment suppressed the NF- κ B pathway in ALDH⁺ and ALDH⁻ cells, the downstream genes were different. About 71% of NF- κ B targets (65/91 genes) were lower and 29% of targets (26/91 genes) were higher in ALDH⁺ cells compared with those in ALDH⁻ cells following DiOC5(3) treatment.

4. Discussion

Twenty-five years ago, Rhodamine 123, a mitochondrial staining fluorescent dye, was shown to selectively kill cancer cells and not normal epithelial cells [39]. Since that discovery, several fluorophores have been demonstrated to behave as indicators/inhibitors of cancer cells and cancer stem-like cells, and these discoveries have been driven by the demand for rapid cancer

diagnosis and evaluation of drug responses in the clinical setting [40]. For example, 8-azaadenosine inhibited ovarian cancer stem-like cells associated with mitotic cellular responses [41], and near-infrared chemicals NIR-780/783 are now being tried as reagents for targeting and selective imaging of cancer cells [21] and stem cells [22]. In this study using our cancer-zebrafish screening method [14], the single molecule DiOC5(3) was shown to behave as both a selective LSC indicator and inhibitor.

4.1. Mechanism of LSC-selective mitochondrial accumulation of DiOC5(3)

DiOC5(3) is a membrane potential-dependent dye and can be used for vital staining of lymphocytes in fluorescence-activated cell sorting [41,42]. This lipophilic cationic carbocyanine was weakly

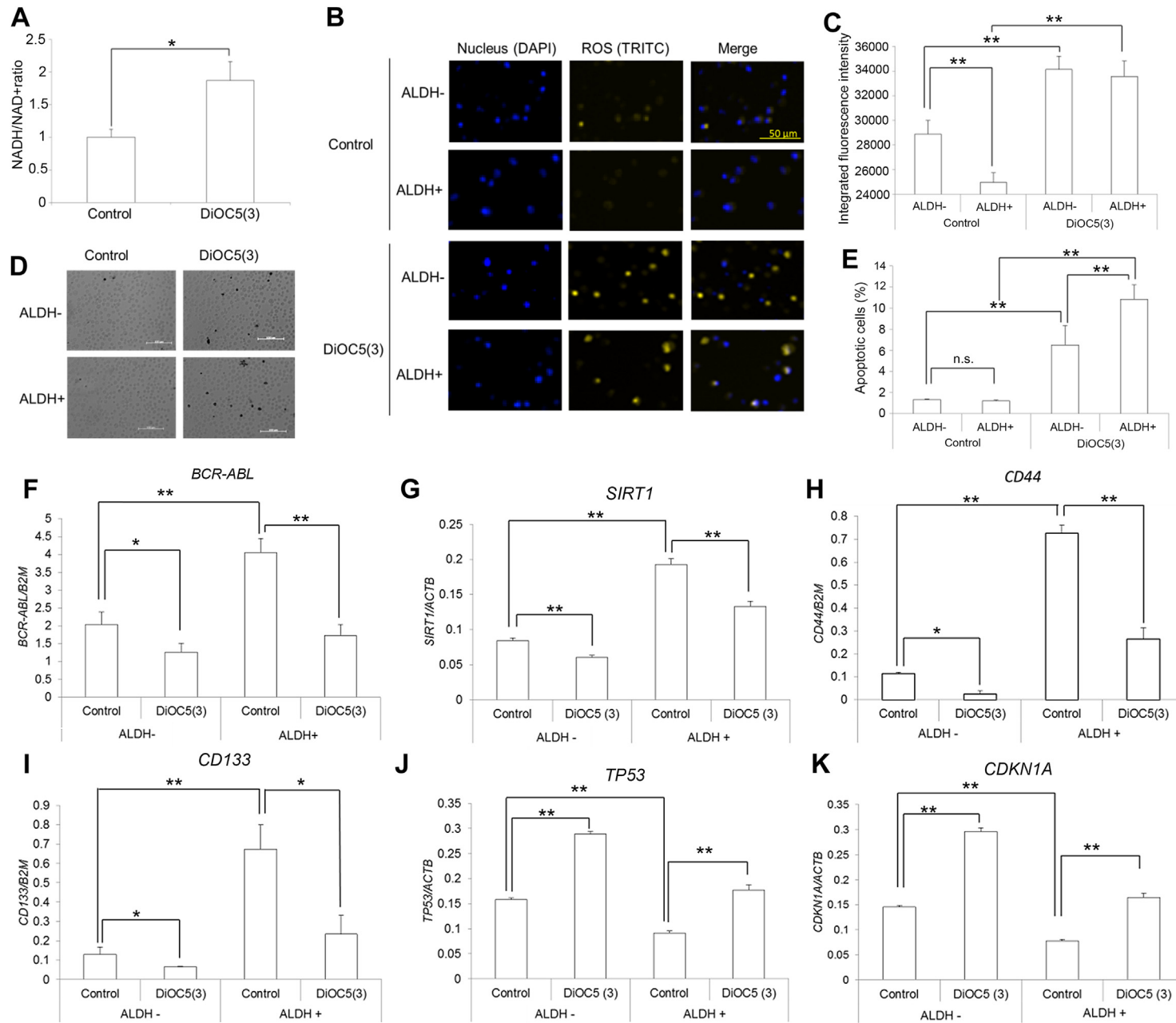


Fig. 4. DiOC5(3) induces apoptosis following ROS overproduction in ALDH⁺ cells. (A) DiOC5(3) (200 nM, 24 h) increased the NADH/NAD⁺ ratio in isolated mitochondria from K562 cells. $n = 3$, $^*P < 0.05$. (B) Representative images of intracellular ROS in K562 ALDH^{-/+} cells without or with DiOC5(3) treatment (200 nM, 24 h). The DAPI filter is for nuclei staining by Hoechst 33342, and the TRITC filter is for the ROS. (C) Quantification of ROS level. ROS of ALDH⁺ cells was lower than that of ALDH⁻ cells, while DiOC5(3) treatment increased ROS in both subpopulations. $n = 4$, $^{**}P < 0.01$. (D) Representative images of apoptotic cells without or with DiOC5(3) treatment (200 nM, 24 h) in K562 ALDH^{-/+} cells. The dark spots indicated the apoptotic cells. (E) Quantification of apoptotic cells. The ALDH⁺ cells exhibited more sensitivity to DiOC5(3) than ALDH⁻ cells in apoptotic response. $n = 4$, n.s., not significant; $^{***}P < 0.01$. (F–I) The expressions of *BCR-ABL* (F), *SIRT1* (G), *CD44* (H) and *CD133* (I) were increased in ALDH⁺ cells and DiOC5(3) treatment (200 nM, 24 h) suppressed them in K562 ALDH^{-/+} cells. $n = 3$, $^*P < 0.05$, $^{**}P < 0.01$. (J,K) The expressions of *TP53* (J) and its down-stream gene *CDKN1A* (K) were decreased in ALDH⁺ cells, and DiOC5(3) treatment (200 nM, 24 h) promoted their expression in K562 ALDH^{-/+} cells. $n = 3$, $^{**}P < 0.01$.

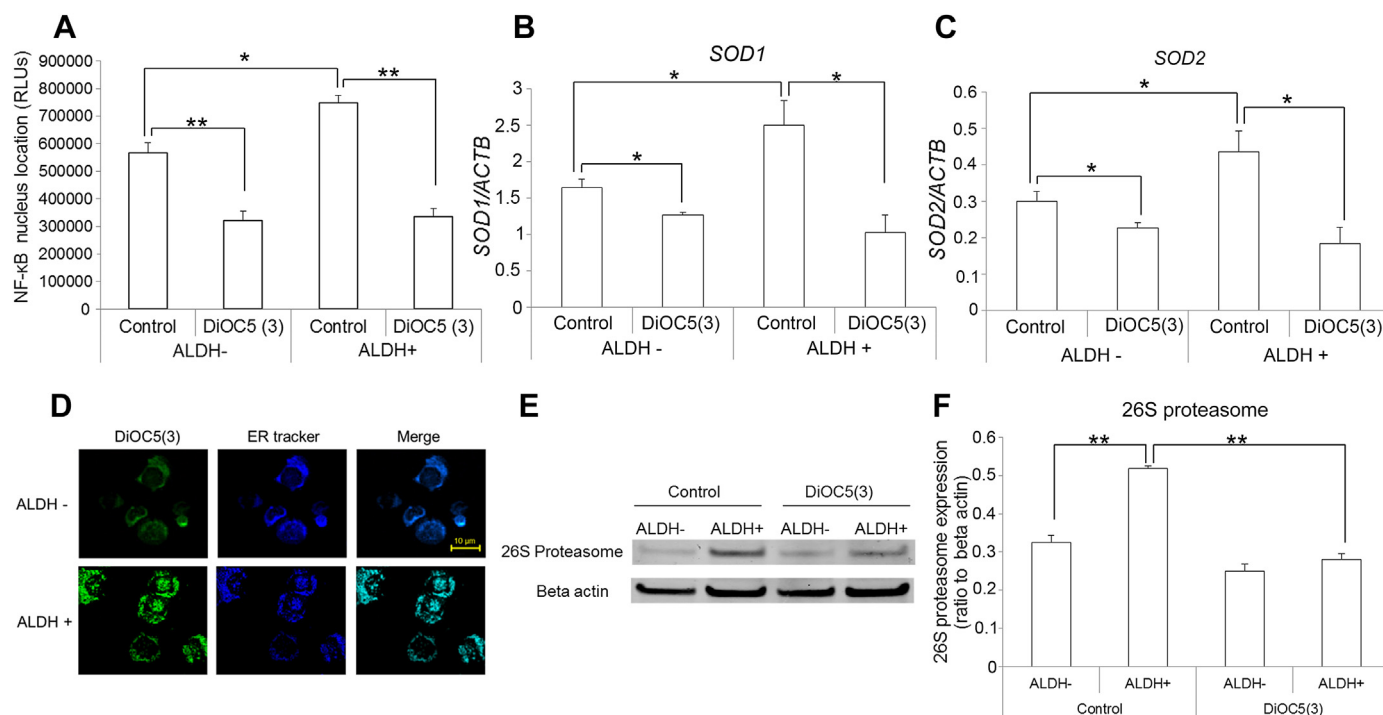


Fig. 5. DiOC5(3) inhibits NF- κ B activity. (A) DiOC5(3) treatment (200 nM, 24 h) inhibited NF- κ B nuclear translocation in ALDH+ cells more than that in ALDH- cells. $n = 3$, $^*P < 0.05$, $^{**}P < 0.01$. (B,C) NF- κ B downstream genes *SOD1* (B) and *SOD2* (C) were highly expressed in ALDH+ cells and downregulated by DiOC5(3) treatment (200 nM, 24 h). $n = 3$, $^*P < 0.05$. (D) Confocal images of ALDH-/+ cells with DiOC5(3) (green) and ER-Tracker Blue-White DPX (blue). In ALDH+ cells, DiOC5(3) and ER-Tracker Blue-White were highly co-localized (cyan) in endoplasmic reticulum. (E) Western blot for the 26S proteasome without or with DiOC5(3) treatment (200 nM, 24 h). (F) Quantification of the Western blot. In ALDH+ cells, 26S proteasome protein was reduced by DiOC5(3) treatment. $n = 3$, $^{**}P < 0.01$. (For interpretation of the references to color in this figure legend, the reader is referred to the web version of this article.)

fluorescent in water but highly fluorescent and quite photostable when incorporated into membranes [3,37]. Once applied to the cells, the dye preferentially diffuses within the plasma membrane and ER in a short time [37]. In general, the lipophilic cations possess a delocalized positive charge, which can penetrate the hydrophobic barriers of the plasma and mitochondrial membranes in response to the negative internal transmembrane potentials [43,44]. The cation DiOC5(3) efficiently incorporates into the cytosol of cancer cells compared with normal cells. However, we found that expression of the LSC-specific OATPs, *SLCO4A1* and *SLCO4C1*, were involved in plasma membrane transport of DiOC5(3). OATPs play an important role in the absorption, distribution, and excretion of many endogenous and exogenous chemicals via the cell membrane, and thus they serve as potential therapeutic targets including cancer [45]. Of these, *SLCO4A1* was highly expressed in leukemia and many other cancer types, but not expressed in normal blood cells [46]. Because of the absence of *SLCO4A1* in the normal blood cells, DiOC5(3) could not be incorporated and exhibited weak cytotoxicity to these cells. Regarding *SLCO4C1*, to the best of our knowledge, this is the first report of its selective expression in LSCs, and may also be involved in the LSC-selectivity of DiOC5(3).

After the incorporation inside cells, DiOC5(3) accumulated in mitochondria and exhibited ROS overproduction. Several studies reported that high mitochondrial membrane potential was present in CSCs compared with non-CSCs and their counterparts of non-malignant cells [47–49]. As a cation dye, DiOC5(3) may also prefer the high mitochondrial membrane potential of LSCs. Because of the dual properties in LSCs of OATP expression and high mitochondrial membrane potential, DiOC5(3) can act as a selective label for LSCs and it exhibits LSC-selective cytotoxicity. In addition, it exhibits passive diffusion as a lipophilic molecule.

4.2. Similar structures to DiOC5(3)

Of the DiOC5(3) analogs, the long carbon chains and long bridge distance between two rings enhance cytotoxicity, except in the case of DiOC18(3). DiOC18(3) may not penetrate the plasma membrane (without fluorescent staining) because of its long carbon chain. In addition, when the last -CH₃ of carbon chains in DiOC5(3) was changed to -COOH, the cytotoxicity was also decreased. This suggests that the carboxylic acid may provide a cation causing DiOC5(3) to accumulate in the mitochondrial membrane, as described above.

4.3. DiOC5(3)-induced ROS killed LSCs

A major source of ROS is the mitochondria, which have been emerging as highly intriguing organelles showing promise for use as targets for anticancer drugs [50]. Moderate levels of ROS result in transient cellular alterations including tumorigenesis, whereas higher levels of ROS, which are sometimes induced by anticancer drug treatment similar to DiOC5(3), result in cell death and/or apoptosis [51–53]. In the previous study, DiOC5(3) was a hyperthermic sensitizer of Chinese hamster ovary (CHO) cells at 43.0 or 45.5 °C, which showed DNA damage, whereas it exhibited no cytotoxicity at 37 °C [34]. Different from the result of CHO cells, DiOC5(3) was able to kill K562 cells at 37 °C because of ROS overproduction, but did not have a cytotoxic effect on normal cells. In comparison to normal cells, malignant cells usually function with higher levels of endogenous oxidative stress [54,55], similar to leukemia cells freshly isolated from patients [56]. Inhibition of NAD⁺ synthesis, probably due to the reductase inactivation by DiOC5(3), likely caused the apoptosis observed in K562 cells,

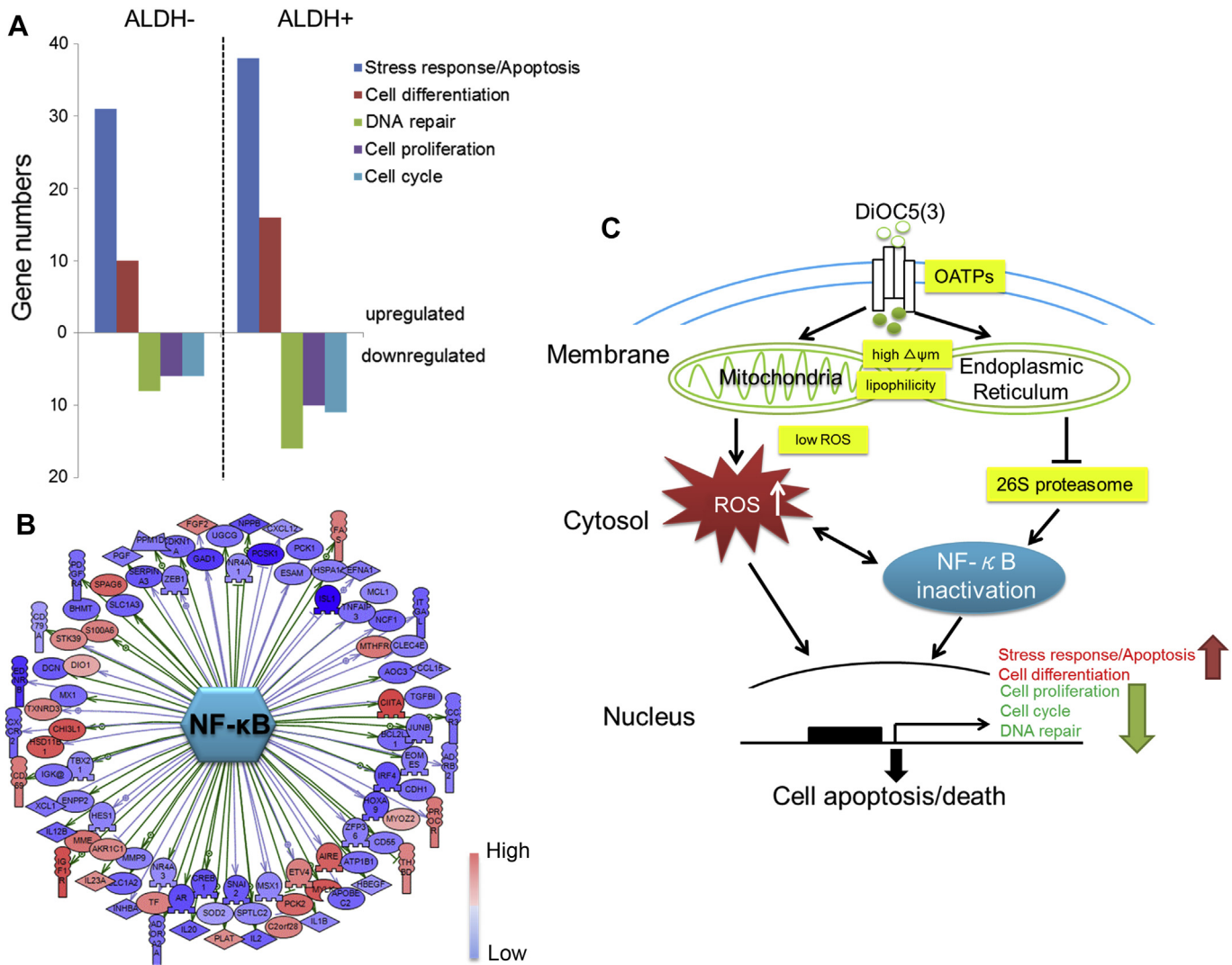


Fig. 6. Transcriptome analysis of DiOC5(3) effects in ALDH+ cells. (A) The gene ontology analysis of altered genes with DiOC5(3) treatment (200 nM, 24 h) in K562 ALDH^{-/+} cells. (B) DiOC5(3) treatment induced different gene expression profiles of NF- κ B pathway in K562 ALDH⁺ cells compared with that of ALDH⁻ cells analyzed by the Sub-Network Enrichment Analysis (SNEA) method. (C) Proposed mechanism of DiOC5(3) action against LSCs. The factors involved in LSC-selectivity of DiOC5(3) are marked with a yellow background. (For interpretation of the references to color in this figure legend, the reader is referred to the web version of this article.)

similar to previous studies [57] including one that examined leukemia [28]. Low ROS levels have been associated with radiotherapy-resistance, suggesting that the involvement of an enhanced ROS defense system exists in CSCs [58]. Because the CSC environment would be more sensitive to oxidative stress than that in normal cancer cells, once the balance was broken between ROS scavenging and production, CSCs were subsequently killed selectively [51]. The LSC subset of K562 cells also contained lower ROS levels than non-LSCs in our study. The high levels of ROS induced by DiOC5(3) might be a trigger for the specific eradication of LSCs, and not non-LSCs and other normal cells, like the synthetic retinoid derivative, fenretinide, against AML stem cells [24].

4.4. DiOC5(3) inhibited NF- κ B activity in LSCs

Aside from being a ROS inducer, we found that DiOC5(3) also suppressed NF- κ B signaling in K562 cells. Constitutive activation of NF- κ B is frequently observed in human cancers of diverse origins and plays a role in oncogenesis [59], angiogenesis and metastasis [60], chemotherapy resistance [61], and survival of CSCs [62]. Thus,

NF- κ B and members of its signaling network are now becoming powerful targets in chemotherapies [63]. There are two signaling pathways leading to the activation of NF- κ B known as the canonical (or classical) pathway and the non-canonical (or alternative) pathway [64,65]. The canonical pathway is required for the induction and maintenance of the epithelial-mesenchymal transition, a process tightly correlated with cancer progression in CSCs [64,66,67]. In the current study, NF- κ B1 mRNA, which participated in the canonical NF- κ B pathway, was significantly higher than NF- κ B2 mRNA in K562 ALDH⁺ but not in ALDH⁻ cells ($P < 0.01$; Supplementary Fig. S7C). In addition, DiOC5(3) and other selective inhibitors of the IKK complex that are involved in the canonical NF- κ B pathway inhibited LSC proliferation selectively in the same way ($P < 0.01$; Supplementary Fig. S7F and G). These data indicate that DiOC5(3) may suppress the canonical NF- κ B pathway, which acts as a main pathway in LSC.

The ER is a multifunctional organelle that plays a central role in many essential cellular activities, such as folding, assembly and quality control of secretory and membrane proteins. Under stress conditions, the ER directly communicates with mitochondria

through close contacts referred to as mitochondria-associated membranes, and subsequently changes secretory protein synthesis rates, unfolds or misfolds proteins and produces ROS [68,69]. DiOC5(3)-induced 26S proteasome downregulation would inhibit the I κ B α ubiquitination and degradation processes after its phosphorylation by IKK α / β / γ subunits (IKK complex), subsequently leading to the inactivation of the canonical NF- κ B pathway [70,71]. In addition, there is also intimate crosstalk between NF- κ B and ROS [32]. The inhibition of NF- κ B led to an increase in ROS levels and to cell death in CML [72]. Conversely, ROS influenced the DNA binding properties of the NF- κ B proteins and regulated NF- κ B activating pathways, resulting in suppression of NF- κ B activity [32]. In fact, some anti-LSC chemicals, such as TDZD-8 and niclosamide, exhibit dual activities including NF- κ B inhibition and ROS overproduction to induce apoptosis in LSCs [29,30], similar to DiOC5(3).

The inactivation of NF- κ B upregulates the downstream genes, *TP53* and *CDKN1A* [73], which were also upregulated by DiOC5(3) in our result. From our transcriptome analysis, expression of several stress-related *TP53* downstream gene was altered by DiOC5(3), including *DDIT3* (*DNA-damage inducible transcript 3*) and *GADD45* (*growth arrest and DNA damage inducible gene 45*). *DDIT3* is activated by ER stress, and promotes apoptosis [74,75]. *GADD45* also plays essential roles in tumor growth suppression related to cell apoptosis [76,77]. Furthermore, *TP53* with ROS accumulation negatively regulates SIRT1, which protects the stem cells as an NAD⁺-dependent deacetylase against ROS accumulation [78,79]. SIRT1 inhibition can also activate *TP53*, which enhances elimination of CML LSCs in combination with imatinib [78]. DiOC5(3) downregulated NF- κ B downstream gene expression, including *SOD1*, *SOD2* and *MMP9* (matrix metalloproteinase 9), and upregulated downstream gene expressions, such as *CIITA* (class II, major histocompatibility complex, transactivator). The *SOD* genes, especially *SOD2*, are responsible for destroying ROS in breast cancer [80], and thus the reduction of SODs may lead LSCs to ROS-induced cell death [81]. *MMP9* is a well-known promoter in cancer metastasis and its reduction may prevent cell migration [82], which was shown in another zebrafish cancer study [13]. Decreased *CIITA* expression is observed in multiple tumor types, and its overexpression induces tissue disorganization allowing cancer cells to evade immune cell-induced apoptosis [83,84].

Conclusion

Using the zebrafish cancer screening method, we found that a fluorescent compound, DiOC5(3), selectively labeled and eradicated LSCs. Owing to the overexpressed OATPs, high membrane potential, and lipophilicity, DiOC5(3) was rapidly incorporated into the cytosol of LSCs, and subsequently accumulated in mitochondria, leading to ROS overproduction that destroyed the low ROS stemness in LSCs. DiOC5(3) also accumulated in the ER leading to the dysfunction of the 26S proteasome overexpressed in LSCs, which likely interfered with the ubiquitination and degradation processes that accompany the activation of the canonical NF- κ B pathway. Fig. 6C shows the predicted mechanism of DiOC5(3)-induced cytotoxicity against LSCs. As the model shows, the dual targeting of both mitochondria and the NF- κ B signaling pathway with a single molecule should play a prominent role in cancer therapy related to cancer stemness.

Funding sources

This work was supported in part by the Japan Science and Technology Agency, KAKENHI of Grants-in-Aid for Scientific Research, and the New Energy and Industrial Technology Development Organization.

Author contributions

T.T., Y.S. and T.M. conceived and designed the study. T.N., T.S., and T.M. synthesized fluorescent chemicals. B.Z., J.K., M.A., T.N., and N.U. performed experiments. B.Z., Y.S., T.S., and Y.N. analyzed the data. B.Z. and Y.S. wrote the paper.

Disclosure of potential conflict of interest

The authors declare that they have no financial or commercial conflict of interest.

Acknowledgments

We thank S. Ichikawa for her assistance in the experiments and the breeding of fish. We also thank R. Ikeyama and Y. Tamura for secretarial assistance.

Appendix A. Supplementary data

Supplementary data related to this article can be found at <http://dx.doi.org/10.1016/j.biomaterials.2015.02.009>.

References

- [1] Stuart SA, Minami Y, Wang JY. The CML stem cell: evolution of the progenitor. *Cell Cycle* 2009;8:1338–43.
- [2] Crews LA, Jamieson CH. Selective elimination of leukemia stem cells: hitting a moving target. *Cancer Lett* 2013;338:15–22.
- [3] Savona M, Talpaz M. Getting to the stem of chronic myeloid leukaemia. *Nat Rev Cancer* 2008;8:341–50.
- [4] Gerber JM, Qin L, Kowalski J, Smith BD, Griffin CA, Vala MS, et al. Characterization of chronic myeloid leukemia stem cells. *Am J Hematol* 2011;86:31–7.
- [5] Fleischman AG. ALDH marks leukemia stem cell. *Blood* 2012;119:3376–7.
- [6] Zon LI, Peterson RT. *In vivo* drug discovery in the zebrafish. *Nat Rev Drug Discov* 2005;4:35–44.
- [7] Murphey RD, Zon LI. Small molecule screening in the zebrafish. *Methods* 2006;39:255–61.
- [8] Taylor AM, Zon LI. Zebrafish tumor assays: the state of transplantation. *Zebrafish* 2009;6:339–46.
- [9] Ghotra VP, He S, de Bont H, van der Ent W, Spaink HP, van de Water B, et al. Automated whole animal bio-imaging assay for human cancer dissemination. *PLoS One* 2012;7: e31281.
- [10] Snaar-Jagalska BE. ZF-CANCER: developing high-throughput bioassays for human cancers in zebrafish. *Zebrafish* 2009;6:441–3.
- [11] Haldi M, Ton C, Seng WL, McGrath P. Human melanoma cells transplanted into zebrafish proliferate, migrate, produce melanin, form masses and stimulate angiogenesis in zebrafish. *Angiogenesis* 2006;9:139–51.
- [12] Eguiara A, Holgado O, Beloqui I, Abalde L, Sanchez Y, Callol C, et al. Xenografts in zebrafish embryos as a rapid functional assay for breast cancer stem-like cell identification. *Cell Cycle* 2011;10:3751–7.
- [13] Yang XJ, Cui W, Gu A, Xu C, Yu SC, Li TT, et al. A novel zebrafish xenotransplantation model for study of glioma stem cell invasion. *PLoS One* 2013;8:e61801.
- [14] Zhang B, Shimada Y, Kuroyanagi J, Umemoto N, Nishimura Y, Tanaka T. Quantitative phenotyping-based *in vivo* chemical screening in a zebrafish model of leukemia stem cell xenotransplantation. *PLoS One* 2014;9:e85439.
- [15] Zhang B, Shimada Y, Kuroyanagi J, Nishimura Y, Umemoto N, Nomoto T, et al. Zebrafish xenotransplantation model for cancer stem-like cell study and high-throughput screening of inhibitors. *Tumour Biol* 2014;35:11861–9.
- [16] Bunting JR, Phan TV, Kamali E, Dowben RM. Fluorescent cationic probes of mitochondria. Metrics and mechanism of interaction. *Biophys J* 1989;56:979–93.
- [17] Rashid F, Horobin RW, Williams MA. Predicting the behaviour and selectivity of fluorescent probes for lysosomes and related structures by means of structure-activity models. *Histochem J* 1991;23:450–9.
- [18] Nishimura Y, Yata K, Nomoto T, Ogiwara T, Watanabe K, Shintou T, et al. Identification of a novel indoline derivative for *in vivo* fluorescent imaging of blood-brain barrier disruption in animal models. *ACS Chem Neurosci* 2013;4:1183–93.
- [19] Watanabe K, Nishimura Y, Nomoto T, Umemoto N, Zhang Z, Zhang B, et al. *In vivo* assessment of the permeability of the blood-brain barrier and blood-retinal barrier to fluorescent indoline derivatives in zebrafish. *BMC Neurosci* 2012;13:101.

- [20] Watanabe K, Nishimura Y, Oka T, Nomoto T, Kon T, Shintou T, et al. *In vivo* imaging of zebrafish retinal cells using fluorescent coumarin derivatives. *BMC Neurosci* 2010;11:116.
- [21] Liu J, Li J, Zhang JF, Xin XY. Combination of fenretinide and selenite inhibits proliferation and induces apoptosis in ovarian cancer cells. *Int J Mol Sci* 2013;14:21790–804.
- [22] Du Y, Xia Y, Pan X, Chen Z, Wang A, Wang K, et al. Fenretinide targets chronic myeloid leukemia stem/progenitor cells by regulation of redox signaling. *Antioxid Redox Signal* 2014;20:1866–80.
- [23] Westerfield M. *The zebrafish book: a guide for the laboratory use of zebrafish danio (branchydanio) rerio*. fifth ed. Eugene: Univ. of Oregon Press; 2007.
- [24] Zhang H, Mi JQ, Fang H, Wang Z, Wang C, Wu L, et al. Preferential eradication of acute myelogenous leukemia stem cells by fenretinide. *Proc Natl Acad Sci U S A* 2013;110:5606–11.
- [25] Oka T, Nishimura Y, Zang L, Hirano M, Shimada Y, Wang Z, et al. Diet-induced obesity in zebrafish shares common pathophysiological pathways with mammalian obesity. *BMC Physiol* 2010;10:21.
- [26] Anderson WM, Wood JM, Anderson AC. Inhibition of mitochondrial and *Paracoccus* denitrificans NADH-ubiquinone reductase by oxacarboxyanine dyes. A structure-activity study. *Biochem Pharmacol* 1993;45:2115–22.
- [27] van Jaarsveld H, Potgieter GM, Lochner A. Changes in NADH-ubiquinone reductase (complex I) with autolysis in the rat heart as experimental model. *Enzyme* 1986;35:206–14.
- [28] dos Santos GA, Abreu e Lima RS, Pestana CR, Lima AS, Scheucher PS, Thome CH, et al. (+)alpha-Tocopheryl succinate inhibits the mitochondrial respiratory chain complex I and is as effective as arsenic trioxide or ATRA against acute promyelocytic leukemia *in vivo*. *Leukemia* 2012;26:451–60.
- [29] Guzman ML, Li X, Corbett CA, Rossi RM, Bushnell T, Liesveld JL, et al. Rapid and selective death of leukemia stem and progenitor cells induced by the compound 4-benzyl, 2-methyl, 1,2,4-thiadiazolidine, 3,5 dione (TDZD-8). *Blood* 2007;110:4436–44.
- [30] Jin Y, Lu Z, Ding K, Li J, Du X, Chen C, et al. Antineoplastic mechanisms of niclosamide in acute myelogenous leukemia stem cells: inactivation of the NF-kappaB pathway and generation of reactive oxygen species. *Cancer Res* 2010;70:2516–27.
- [31] Deng CH, Zhang QP. Leukemia stem cells in drug resistance and metastasis. *Chin Med J* 2010;123:954–60.
- [32] Morgan MJ, Liu ZG. Crosstalk of reactive oxygen species and NF-kappaB signaling. *Cell Res* 2011;21:103–15.
- [33] Barre B, Coqueret O, Perkins ND. Regulation of activity and function of the p52 NF-kappaB subunit following DNA damage. *Cell Cycle* 2010;9:4795–804.
- [34] Borrelli MJ, Rausch CM, Seaner R, Iliakis G. Sensitization to hyperthermia by 3,3'-dipentylloxycarbonyl iodide: a positive correlation with DNA damage and negative correlations with altered cell morphology, oxygen consumption inhibition, and reduced ATP levels. *Int J Hypertherm Off J Eur Soc Hyperthermic Oncol North Am Hypertherm Group* 1991;7:243–61.
- [35] Burke JR, Pattoli MA, Gregor KR, Brassil PJ, MacMaster JF, McIntyre KW, et al. BMS-345541 is a highly selective inhibitor of I kappa B kinase that binds at an allosteric site of the enzyme and blocks NF-kappa B-dependent transcription in mice. *J Biol Chem* 2003;278:1450–6.
- [36] Gaurnier-Hausser A, Patel R, Baldwin AS, May MJ, Mason NJ. NEMO-binding domain peptide inhibits constitutive NF-kappaB activity and reduces tumor burden in a canine model of relapsed, refractory diffuse large B-cell lymphoma. *Clin Cancer Res Off J Am Assoc Cancer Res* 2011;17:4661–71.
- [37] Tscherepanow M, Jensen N, Kummert F. An incremental approach to automated protein localisation. *BMC Bioinformatics* 2008;9:445.
- [38] Kotelnikova E, Yuryev A, Mazo I, Daraselia N. Computational approaches for drug repositioning and combination therapy design. *J Bioinform Comput Biol* 2010;8:593–606.
- [39] Modica-Napolitano JS, Aprille JR. Basis for the selective cytotoxicity of rhodamine 123. *Cancer Res* 1987;47:4361–5.
- [40] Sutton EJ, Henning TD, Pichler BJ, Bremer C, Daldrup-Link HE. Cell tracking with optical imaging. *Eur Radiol* 2008;18:2021–32.
- [41] Mezenecv R, Wang L, McDonald JF. Identification of inhibitors of ovarian cancer stem-like cells by high-throughput screening. *J Ovarian Res* 2012;5:30.
- [42] Wiczorek K, Niewiarowska J. Cancer stem cells. *Postepy Hig Med Dosw (Online)* 2012;66:629–36.
- [43] Johnson LV, Walsh ML, Bockus BJ, Chen LB. Monitoring of relative mitochondrial membrane potential in living cells by fluorescence microscopy. *J Cell Biol* 1981;88:526–35.
- [44] Chen LB. Mitochondrial membrane potential in living cells. *Annu Rev Cell Biol* 1988;4:155–81.
- [45] Obaidat A, Roth M, Hagenbuch B. The expression and function of organic anion transporting polypeptides in normal tissues and in cancer. *Annu Rev Pharmacol Toxicol* 2012;52:135–51.
- [46] Tamai I, Nezu J, Uchino H, Sai Y, Oka A, Shimane M, et al. Molecular identification and characterization of novel members of the human organic anion transporter (OATP) family. *Biochem Biophys Res Commun* 2000;273:251–60.
- [47] Hockenbery DM. A mitochondrial achilles' heel in cancer? *Cancer Cell* 2002;2:1–2.
- [48] Ye XQ, Li Q, Wang GH, Sun FF, Huang GJ, Bian XW, et al. Mitochondrial and energy metabolism-related properties as novel indicators of lung cancer stem cells. *Int J Cancer* 2011;129:820–31.
- [49] Ye XQ, Wang GH, Huang GJ, Bian XW, Qian GS, Yu SC. Heterogeneity of mitochondrial membrane potential: a novel tool to isolate and identify cancer stem cells from a tumor mass? *Stem Cell Res* 2011;7:153–60.
- [50] Rohlena J, Dong LF, Ralph SJ, Neuzil J. Anticancer drugs targeting the mitochondrial electron transport chain. *Antioxid Redox Signal* 2011;15:2951–74.
- [51] Abdel-Wahab O, Levine RL. Metabolism and the leukemic stem cell. *J Exp Med* 2010;207:677–80.
- [52] Tothova Z, Gilliland DG. FoxO transcription factors and stem cell homeostasis: insights from the hematopoietic system. *Cell Stem Cell* 2007;1:140–52.
- [53] Trachootham D, Alexandre J, Huang P. Targeting cancer cells by ROS-mediated mechanisms: a radical therapeutic approach? *Nat Rev Drug Discov* 2009;8:579–91.
- [54] Szatrowski TP, Nathan CF. Production of large amounts of hydrogen peroxide by human tumor cells. *Cancer Res* 1991;51:794–8.
- [55] Kawanishi S, Hiraku Y, Pinlaor S, Ma N. Oxidative and nitrate DNA damage in animals and patients with inflammatory diseases in relation to inflammation-related carcinogenesis. *Biol Chem* 2006;387:365–72.
- [56] Zhou Y, Hileman EO, Plunkett W, Keating MJ, Huang P. Free radical stress in chronic lymphocytic leukemia cells and its role in cellular sensitivity to ROS-generating anticancer agents. *Blood* 2003;101:4098–104.
- [57] Muruganandham M, Alfieri AA, Matei C, Chen Y, Sukenick G, Schemainda I, et al. Metabolic signatures associated with a NAD synthesis inhibitor-induced tumor apoptosis identified by 1H-decoupled-31P magnetic resonance spectroscopy. *Clin Cancer Res Off J Am Assoc Cancer Res* 2005;11:3503–13.
- [58] Diehn M, Cho RW, Lobo NA, Kalisky T, Dorie MJ, Kulp AN, et al. Association of reactive oxygen species levels and radioresistance in cancer stem cells. *Nature* 2009;458:780–3.
- [59] Basseres DS, Baldwin AS. Nuclear factor-kappaB and inhibitor of kappaB kinase pathways in oncogenic initiation and progression. *Oncogene* 2006;25:6817–30.
- [60] Prasad S, Ravindran J, Aggarwal BB. NF-kappaB and cancer: how intimate is this relationship. *Mol Cell Biochem* 2010;336:25–37.
- [61] Sakamoto K, Maeda S. Targeting NF-kappaB for colorectal cancer. *Expert Opin Ther Targets* 2010;14:593–601.
- [62] Zhou J, Zhang H, Gu P, Bai J, Margolick JB, Zhang Y. NF-kappaB pathway inhibitors preferentially inhibit breast cancer stem-like cells. *Breast Cancer Res Treat* 2008;111:419–27.
- [63] Hoesele B, Schmid JA. The complexity of NF-kappaB signaling in inflammation and cancer. *Mol Cancer* 2013;12:86.
- [64] Shostak K, Chariot A. NF-kappaB, stem cells and breast cancer: the links get stronger. *Breast cancer research. BCR* 2011;13:214.
- [65] Biswas DK, Shi Q, Baily S, Strickland I, Ghosh S, Pardee AB, et al. NF-kappa B activation in human breast cancer specimens and its role in cell proliferation and apoptosis. *Proc Natl Acad Sci U S A* 2004;101:10137–42.
- [66] Huber MA, Azoitei N, Baumann B, Grunert S, Sommer A, Pehamberger H, et al. NF-kappaB is essential for epithelial-mesenchymal transition and metastasis in a model of breast cancer progression. *J Clin Invest* 2004;114:569–81.
- [67] Liu M, Sakamaki T, Casimiro MC, Willmarth NE, Quong AA, Ju X, et al. The canonical NF-kappaB pathway governs mammary tumorigenesis in transgenic mice and tumor stem cell expansion. *Cancer Res* 2010;70:10464–73.
- [68] Giorgi C, De Stefani D, Bononi A, Rizzuto R, Pinton P. Structural and functional link between the mitochondrial network and the endoplasmic reticulum. *Int J Biochem Cell Biol* 2009;41:1817–27.
- [69] Breckenridge DG, Germain M, Mathai JP, Nguyen M, Shore GC. Regulation of apoptosis by endoplasmic reticulum pathways. *Oncogene* 2003;22:8608–18.
- [70] Hu X. Proteolytic signaling by TNFalpha: caspase activation and IkkappaB degradation. *Cytokine* 2003;21:286–94.
- [71] Fuster V, Ryden LE, Cannon DS, Crijns HJ, Curtis AB, Ellenbogen KA, et al. ACC/AHA/ESC 2006 guidelines for the management of patients with atrial fibrillation—executive summary. *Rev Port Cardiol* 2007;26:383–446.
- [72] Stein SJ, Baldwin AS. NF-kappaB suppresses ROS levels in BCR-ABL(+) cells to prevent activation of JNK and cell death. *Oncogene* 2011;30:4557–66.
- [73] Kaltschmidt B, Kaltschmidt C, Hehner SP, Droge W, Schmitz ML. Repression of NF-kappaB impairs HeLa cell proliferation by functional interference with cell cycle checkpoint regulators. *Oncogene* 1999;18:3213–25.
- [74] Suresh A, Subedi K, Kyathanahalli C, Jeyasuria P, Condon JC. Uterine endoplasmic reticulum stress and its unfolded protein response may regulate caspase 3 activation in the pregnant mouse uterus. *PLoS One* 2013;8:e75152.
- [75] Jauhainen A, Thomsen C, Strombom L, Grundevik P, Andersson C, Danielsson A, et al. Distinct cytoplasmic and nuclear functions of the stress induced protein DDIT3/CHOP/GADD153. *PLoS One* 2012;7:e33208.
- [76] Hwang SG, Park J, Park JY, Park CH, Lee KH, Cho JW, et al. Anti-cancer activity of a novel small molecule compound that simultaneously activates p53 and inhibits NF-kappaB signaling. *PLoS One* 2012;7:e44259.
- [77] Tamura RE, de Vasconcellos JF, Sarkar D, Libermann TA, Fisher PB, Zerbini LF. GADD45 proteins: central players in tumorigenesis. *Curr Mol Med* 2012;12:634–51.
- [78] Li L, Wang L, Wang Z, Ho Y, McDonald T, Holyoake TL, et al. Activation of p53 by SIRT1 inhibition enhances elimination of CML leukemia stem cells in combination with imatinib. *Cancer Cell* 2012;21:266–81.
- [79] Yang LJ, Chen Y, He J, Yi S, Wen L, Zhao S, et al. Effects of gambogic acid on the activation of caspase-3 and downregulation of SIRT1 in RPMI-8226 multiple myeloma cells via the accumulation of ROS. *Oncol Lett* 2012;3:1159–65.
- [80] Papa L, Hahn M, Marsh EL, Evans BS, Germain D. SOD2 to SOD1 switch in breast cancer. *J Biol Chem* 2014;289:5412–6.

- [81] Liu L, Chen R, Huang S, Wu Y, Li G, Liu Q, et al. Knockdown of SOD1 sensitizes the CD34+ CML cells to imatinib therapy. *Med Oncol* 2011;28:835–9.
- [82] Jimenez RE, Hartwig W, Antoniu BA, Compton CC, Warshaw AL, Fernandez-Del Castillo C. Effect of matrix metalloproteinase inhibition on pancreatic cancer invasion and metastasis: an additive strategy for cancer control. *Ann Surg* 2000;231:644–54.
- [83] Truax AD, Thakkar M, Greer SF. Dysregulated recruitment of the histone methyltransferase EZH2 to the class II transactivator (CIITA) promoter IV in breast cancer cells. *PLoS One* 2012;7:e36013.
- [84] Liu A, Takahashi M, Toba K, Zheng Z, Hashimoto S, Nikkuni K, et al. Regulation of the expression of MHC class I and II by class II transactivator (CIITA) in hematopoietic cells. *Hematol Oncol* 1999;17:149–60.